Journal of Materials Chemistry C

PAPER

View Article Online
View Journal | View Issue

Cite this: J. Mater. Chem. C, 2019, 7, 4173

Pressure effect on spin-driven multiferroicity in a Y-type hexaferrite

Kun Zhai, [ab] Na Su,[ac] Jianping Sun,[a] Jinguang Cheng, [acd] Zhongyuan Liu[b] and Young Sun *[acd]

Received 25th January 2019,
Accepted 8th March 2019

DOI: 10.1039/c9tc00477g

rsc.li/materials-c

We have investigated the influence of pressure on the magnetoelectric multiferroicity of the $Ba_{1.5}Sr_{0.5}Mg_2Fe_{12}O_{22}$ hexaferrite under hydrostatic pressures up to 3.08 GPa. The spin-induced ferroelectricity is dramatically suppressed by pressure. The electric polarization and magnetoelectric coefficient at 3.08 GPa are reduced to about half of those at 0.12 GPa. With increasing pressure, the critical magnetic field of the transverse conical to longitudinal conical phase transition shifts toward higher fields and the magnetic phase temperatures shift to lower temperatures, indicating tunable exchange interactions by pressure. The suppression of spin-induced ferroelectricity by pressure in $Ba_{1.5}Sr_{0.5}Mg_2Fe_{12}O_{22}$ is ascribed to the weakening of the inverse Dzyaloshinskii–Moriya interaction based on the spin current model.

I. Introduction

Multiferroic materials with magnetoelectric (ME) effects provide new dimensionalities for the manipulation of magnetization (M) by an electric field (E) and the control of electric polarization (P) by a magnetic field (H), which can be used in the fabrication of next generation, low power consumption, high density memory devices.[1–6] In particular, spin-driven multiferroics showing prominent ME effects attract much attention due to the intrinsic coupling between magnetism and ferroelectricity.[7–9] The polarization in spin-driven multiferroics may originate from the inverse Dzyaloshinskii–Moriya (D–M) interaction, the spin current model (KNB model), d–p hybridization, and exchange striction.[10–13] In the past decade, many spin-induced multiferroics have been discovered, such as binary perovskite manganites Mn_2O_3,[14] hexaferrites,[15,16] the mixed-valence manganese oxide family RMn_2O_5 (R = Y, Tb, Ho, Er or Tm),[17,18] noncentrosymmetric nonpolar tetragonal antiferromagnet $Ba_2CoGe_2O_7$,[13] rare-earth orthoferrites $RFeO_3$ (R = $Dy_{0.70}Tb_{0.30}$, $Dy_{0.75}Gd_{0.25}$),[19] and so on.

The hexaferrites with noncollinear magnetic structures are among the most promising candidates to achieve large ME effects. Hexaferrites can be classified into different types based on the stacking sequence of building blocks, *i.e.*, R block [$(Ba,Sr)Fe_6O_{11}$], T block [$(Ba,Sr)_2Fe_8O_{14}$], and S block ($MeFe_4O_8$). The main types of hexaferrites include M-type [$(Ba,Sr)Fe_{12}O_{19}$], W-type [$(Ba,Sr)Me_2Fe_{16}O_{27}$], X-type [$(Ba,Sr)_2Me_2Fe_{28}O_{46}$], Y-type [$(Ba,Sr)_2Me_2Fe_{12}O_{22}$], Z-type [$(Ba,Sr)_3Me_2Fe_{24}O_{41}$], and U-type [$(Ba,Sr)_4Me_2Fe_{36}O_{60}$].[20–25]

In recent years, physical pressure has been used to modify spin-driven multiferroicity. The ferroelectric phase of rare-earth manganites $RMnO_3$ (R = Dy, Tb, and Gd) shows a drastic change with pressure. T. Aoyama *et al.* reported that high pressure can induce an E-type antiferromagnetic phase that enhances P to 1 μC cm^{-2} in $TbMnO_3$.[26] A large change of P as high as 1.3 μC cm^{-2} at 8.4 GPa was reported in $GdMnO_3$.[27] The pressure-induced enhancement of Gd–Mn and Mn–Mn exchange interactions can strengthen the ferroelectricity of $GdMn_2O_5$.[28] CuO is predicted by calculations to be a room-temperature multiferroic with large polarization under high pressure.[29] In previous studies, we found that the introduction of chemical pressure by partially replacing Ba with smaller Sr in the Y-type hexaferrite $Ba_2Mg_2Fe_{12}O_{22}$ can greatly tune the spin cone symmetry to achieve the highest ME coefficient (α_H = 33 000 ps m^{-1}) in single-phase multiferroics.[30] Compared with chemical pressure induced local distortion and modification of the magnetic structure, physical pressure can uniformly affect the magnetic interaction. However, the influence of physical pressure on the spin-driven multiferroicity of Y-type hexaferrites has not been studied to date.

In this work, we have investigated the evolution of spin-driven ferroelectricity in a Y-type hexaferrite $Ba_{1.5}Sr_{0.5}Mg_2Fe_{12}O_{22}$ with hydrostatic pressures up to 3.08 GPa. Different from the chemical pressure induced giant ME effects, we find

[a] Beijing National Laboratory for Condensed Matter Physics and Beijing Advanced Innovation Center for Material Genome Engineering, Institute of Physics, Chinese Academy of Sciences, Beijing 100190, China. E-mail: youngsun@iphy.ac.cn
[b] Center for High Pressure Science (CHiPs), State Key Laboratory of Metastable Materials Science and Technology, Yanshan University, Qinhuangdao 066004, China
[c] School of Physical Science, University of Chinese Academy of Sciences, Beijing 100190, China
[d] Songshan Lake Materials Laboratory, Dongguan, Guangdong 523808, China

that physical pressure suppresses the ME effects by reducing P. The magnetization measurements reveal that the manipulation of exchange interactions by pressure leads to the decay of spin-induced ferroelectricity.

II. Experiments

A single crystal of $Ba_{1.5}Sr_{0.5}Mg_2Fe_{12}O_{22}$ with nominal content was synthesized from a high temperature Na_2O–Fe_2O_3 flux at 1420 °C in a platinum crucible. Thermal recycling was performed before slowly cooling to 1100 °C.[31] The magnetodielectric and ME currents under hydrostatic pressures up to 3.08 GPa were measured by using a piston cylinder pressure cell in a cryogen-free superconducting magnet system (Oxford Instruments, Teslatron PT). The pressure inside the piston cylinder cell was determined at room temperature from the relative resistance change of a manganin gauge *via* P (kbar) = $\Delta R/R0/0.00251$ and the transmitting medium is Daphne 7373. For the ME current measurements, H was applied along the [100] direction with E along the [120] direction. Before the ME current measurements, an ME poling procedure was performed as follows: $E = 1.2$ MV m^{-1} was applied at $H = 50$ kOe and H was ramped to 0.5 kOe. Subsequently, E was turned off and the sample was shorted for 30 min before sweeping H to obtain the ME currents. The polarization was obtained by integrating the ME currents with time. Magnetization measurements were carried out using a Magnetic Properties Measurement System (MPMS-3, Quantum Design) using a miniature piston pressure cell with Daphne 7373 as the pressure transmitting medium. Pb was loaded into a Teflon capsule together with the sample to calibrate the pressure.

III. Results and discussion

Fig. 1a shows the crystal structure of Y-type hexaferrite $Ba_{1.5}Sr_{0.5}Mg_2Fe_{12}O_{22}$. Fe and Mg randomly occupy the tetrahedral and octahedral sites. Ba^{2+} ions are replaced by smaller Sr^{2+} ions, introducing local lattice distortion.[21] Its space group is $R\bar{3}m$, which does not produce spontaneous electric polarization. Nevertheless, the noncollinear magnetic structure can generate polarization due to the spin current model.[11] The magnetic structure can be divided into two kinds of magnetic blocks, small (S) and large (L) blocks, respectively. L and S blocks alternately stack along the c axis. The magnetic moments of Fe^{3+} align collinearly in each block, while they arrange noncollinearly between blocks. Typically, upon cooling down, the Y-type hexaferrite first forms the proper screw magnetic phase as shown in Fig. 1b. With further decreasing temperature, it enters into the longitudinal cone (LC) magnetic structure (Fig. 1c). When a magnetic field H_{ab} is applied in the ab plane, the magnetic moment rotates along H producing the transverse cone (TC) structure. According to the spin current model, $P \sim A\sum e_{ij} \times (S_i \times S_j)$ (A is proportional to the exchange energy, e_{ij} denotes the vector connecting adjacent spins, and S_{ij}

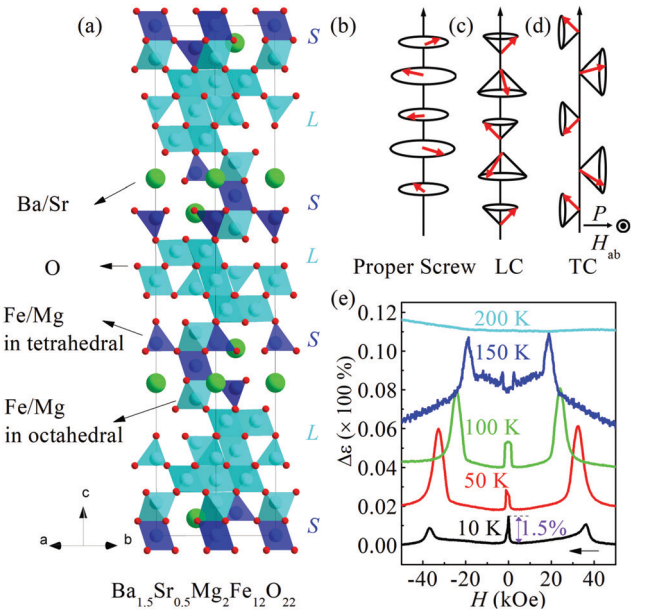

Fig. 1 (a) The crystal structure of Y-type hexaferrite $Ba_{1.5}Sr_{0.5}Mg_2Fe_{12}O_{22}$. (b) The proper screw magnetic structure. (c) The longitudinal cone magnetic structure. (d) The transverse cone magnetic structure. (e) The relative change in the dielectric constant $\Delta\varepsilon = [\varepsilon(H) - \varepsilon(5\text{ kOe})]/\varepsilon(5\text{ kOe})$ with the in-plane magnetic field at selected temperatures. The arrow denotes the direction of the sweeping magnetic field. The curves are shifted vertically for clarity.

represent the magnetic spins),[11] the TC magnetic structure can induce in-plane P as shown in Fig. 1c.

We measured the magnetodielectric behavior at different temperatures (10 K–200 K) with the magnetic field ranging from 50 kOe to −50 kOe at 0 GPa. At 10 K, a broad peak in the low magnetic field region indicates the reversal of P and the change of ε is ∼1.5%. With increasing temperature up to 150 K, the peak broadens and becomes flat and then splits at higher fields, exhibiting a multi-transition feature. At much higher magnetic fields, another peak can also be observed, which indicates the paraelectric (high field) to ferroelectric (low field) phase transition. As the temperature increases, the peak shifts to lower magnetic fields. At 200 K, no obvious features can be seen in the magnetodielectric curves due to the reduced resistance of $Ba_{1.5}Sr_{0.5}Mg_2Fe_{12}O_{22}$ at elevated temperatures.

Then we studied the magnetoelectric properties at 10 K under high pressures up to 3.08 GPa. Fig. 2a shows the schematic setup of the pressure cell and measurement configuration. The polished thin plate sample was loaded into a clamping nut filled with oil (Daphne 7373). By pushing the pusher to compress the volume of the transmission medium, we can obtain a quasi-isostatic pressure environment as high as 3.08 GPa at room temperature. The electric field was applied along the [120] direction and the magnetic field was along the [100] axis. Fig. 2b shows the relative variation of the dielectric constant, $\Delta\varepsilon = [\varepsilon(H) - \varepsilon(5\text{ kOe})]/\varepsilon(5\text{ kOe})$, under selected pressures. At 0.122 GPa, a sharp dielectric peak appears around zero magnetic field, coexisting with a broad shoulder at negative magnetic field. The amplitude of the dielectric peak is merely

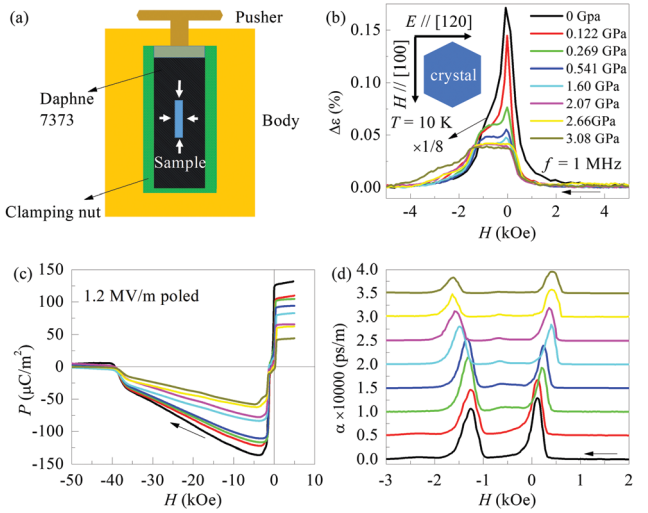

Fig. 2 (a) The schematic configuration of the piston pressure cell with the sample sealed in the clamping nut. (b) The relative change of the dielectric constant with the magnetic field, $\Delta\varepsilon = [\varepsilon(H) - \varepsilon(5\ \text{kOe})]/\varepsilon(5\ \text{kOe})$, under different pressures. The inlet shows the measurement configurations: H is applied along [100] and E is applied along [100]. (c) The variation of spin-induced polarization under different pressures. (d) The magnetoelectric coefficient α_H at 10 K under different pressures. The curves are regularly shifted upward by 5000 ps m^{-1} for a better view. The arrows denote the sweeping direction of the magnetic field.

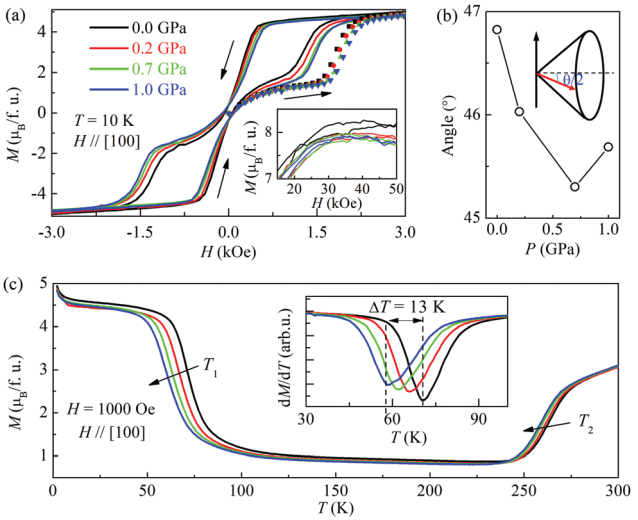

Fig. 3 (a) Magnetic hysteresis loops at 10 K under different pressures. H is along [100]. The inset shows the magnetization curves at higher fields. (b) The estimated transverse cone angle $\theta/2$ as a function of pressure. The angle is derived from the equation $\cos\theta/2 = M_{5\text{kOe}}/M_{50\text{kOe}}$. (c) Temperature dependence of magnetization with H = 1000 Oe under different pressures. H was set to 50 kOe along [100] firstly at T = 2 K and then to 1 kOe and the M–T curve was obtained with slowly warming the sample. The inset shows the differential of magnetization with temperature in the range of 30 K to 100 K.

0.14%, greatly lower than that under ambient pressure (~1.5%). With increased pressure, the dielectric peaks are gradually suppressed. The dielectric peaks become flat when the pressure is 2.07 GPa and change slightly with further increasing pressure. Fig. 2c shows the change of polarization with H after a poling procedure with E = 1.2 MV m^{-1} at 10 K. At ambient pressure the polarization is 128 μC m^{-2}. The polarization is 110 μC m^{-2} at a pressure of 0.122 GPa. The slight change of polarization compared with the greatly depressed dielectric constant at 0.122 GPa may come from different measurement means. For the dielectric measurements it is an AC method sensitive to dissipative dynamics. With the increase of pressure, the polarization gradually decreases, reaching 50 μC m^{-2} at 3.08 GPa, over two times smaller than that under ambient pressure.

Fig. 2d shows the magnetoelectric coefficient (α_H) with the magnetic field ranging from 2 kOe to −3 kOe. The maximum ME coefficient is 12 000 ps m^{-1} at 110 Oe without pressure. At 0.122 GPa, the maximum ME coefficient becomes 11 000 ps m^{-1} at H = 125 Oe. The ME coefficient peak around zero field has a long tail feature, indicating a metamagnetic transition. This transition emerges clearly and shifts to a higher field (along the negative magnetic field direction) with increasing pressure. Besides, the two main ME coefficient peaks at H = 0.12 kOe and H = −1.2 kOe also shift to higher fields (absolute value) with pressure. The change of critical magnetic field for these transitions reaches 400 Oe at 3.08 GPa, indicating that the magnetic property is effectively tuned by high pressures. The ME coefficient is gradually suppressed with increasing pressure. At 3.08 GPa, the maximum ME coefficient is reduced to 5000 ps m^{-1}.

We further studied the magnetic property under high pressures in order to gain an insight into the origin of the pressure effect on multiferroicity. Fig. 3a shows the magnetic hysteresis loops at 10 K under different pressures. The dotted lines outside the hysteresis curves represent the initial magnetization curve, where the rapid increase of magnetization at 1.5 kOe (0 GPa) denotes a magnetic transition from LC to TC. With increasing pressure, the critical magnetic field of the TC to LC transition shifts toward higher fields. The hysteresis loops show a multi-step feature. In the field-sweep-down branch, for 0 GPa, a step decrease of magnetization takes place around 0.1 kOe (denoted as H_1) and −1.3 kOe (denoted as H_2). With increasing pressure, H_1 shifts to positive higher fields and H_2 shifts to negative higher fields, which is consistent with the change of the ME coefficient. The inset in Fig. 3a shows the magnetization curves at high fields under different pressures. The saturation magnetization slightly decreases from 8 μ_B/f.u. at 0 GPa to 7.89 μ_B/f.u., 7.75 μ_B/f.u., and 7.74 μ_B/f.u. at 0.2 GPa, 0.7 GPa, and 1.0 GPa, respectively.

In general, the polarization in hexaferrites is induced by the spin current model, which can be quantitatively described by the relation $P \sim Am_Sm_L \sin\theta/2$.[32] A is determined by the exchange interaction and spin orbital coupling. m_S denotes the magnetic moment of the S block and m_L denotes the magnetic moment of the L block. θ represents the cone opening angle of the LC phase at high fields (two-fold phase), as shown in the inset of Fig. 2b, which is estimated from the equation $\cos\theta/2 = M$ 5 kOe/M 50 kOe.[32] m_S and m_L are nearly invariant due to almost the same saturated magnetization under different pressures. We calculated the value

of $\theta/2$ and summarize it in Fig. 3b. $\theta/2$ decreases with increasing pressure from 0 GPa to 0.7 GPa, but slightly increases at 1 GPa. However, the change of $\theta/2$ is only within the range of 1.5°, which should have a minor influence on the polarization.

Additionally, the pressure induced lattice distortion can affect the magnetic interactions at the boundary of L and S blocks, especially the bond angle and bond distance of super-exchange Fe4–O2–Fe5.[30,33,34] Then we measured the temperature dependence of magnetization with H along the a axis under different pressures. We first apply a saturation magnetic field H = 50 kOe, then set H to 1000 Oe and gradually warm temperature to 300 K. At 0 GPa, we can see a plateau at low temperatures, indicating the TC magnetic phase. The magnetization decreases from 75 K and becomes flat around 110 K, which indicates that the magnetic moments slowly rotate from the ab plane to the c axis, and the TC phase gradually changes to the proper screw magnetic structure. At 240 K, the magnetization starts to increase, which represents the magnetic structure entering into the ferrimagnetic phase. We denote the transition temperature from TC to proper screw as T_1 and proper screw to ferrimagnetic as T_2. With increasing pressure, both T_1 and T_2 shift to lower temperatures, suggesting tunable exchange interactions by pressure in $Ba_{1.5}Sr_{0.5}Mg_2Fe_{12}O_{22}$. We use the derivative of dM/dT to clearly demonstrate the change of T_1 shown in the inset of Fig. 3c. The change of temperature is as large as 13 K from 0 GPa to 1 GPa, signaling the significant tuning effect of magnetic interactions by pressure. In terms of the spin current model $P \sim Am_Sm_L \sin\theta/2$, the pressure seems have little influence on θ, m_S, and m_L. In contrast, the prominent reduction of T_1 reflects the weakening of the exchange interaction, corresponding to the decrease of A. Consequently, the spin-driven electric polarization is suppressed by pressure.

IV. Conclusion

In conclusion, we have studied the influence of pressure on the multiferroicity of $Ba_{1.5}Sr_{0.5}Mg_2Fe_{12}O_{22}$. The spin-driven ferroelectricity is greatly suppressed under high pressure. The magnetization measurements have revealed that the magnetic exchange interaction can be tuned by pressure, which leads to the decrease of the inverse DM interaction. The semiquantitative analyses based on the spin-current model can account for the influence of pressure on the spin-induced ferroelectricity. Though the pressure effect is negative in the $Ba_{1.5}Sr_{0.5}Mg_2Fe_{12}O_{22}$ sample, our study suggests that the spin-driven multiferroicity is sensitive to hydrostatic pressure. An enhancement of the ME effects in some multiferroic hexaferrites could be expected and will be further exploited in the future.

Conflicts of interest

There are no conflicts to declare.

Acknowledgements

This work was supported by the National Natural Science Foundation of China (Grant No. 51725104, 11534015), the National Key Research and Development Program of China (Grant No. 2016YFA0300701, 2018YFA0305700), and Beijing Natural Science Foundation (Grant No. Z180009).

References

1 T. Kimura, T. Goto, H. Shintani, K. Ishizaka, T. Arima and Y. Tokura, *Nature*, 2003, **426**, 55–58.
2 N. A. Spaldin and M. Fiebig, *Science*, 2005, **309**, 391–392.
3 W. Eerenstein, N. D. Mathur and J. F. Scott, *Nature*, 2006, **442**, 759.
4 S.-W. Cheong and M. Mostovoy, *Nat. Mater.*, 2007, **6**, 21–29.
5 J. X. Shen, J. Z. Cong, Y. S. Chai, D. S. Shang, S. P. Shen, K. Zhai, Y. Tian and Y. Sun, *Phys. Rev. Appl.*, 2016, **6**, 021001.
6 K. Zhai, D. S. Shang, Y. S. Chai, G. Li, J. W. Cai, B. G. Shen and Y. Sun, *Adv. Funct. Mater.*, 2018, **28**, 1705771.
7 Y. Tokura, S. Seki and N. Nagaosa, *Rep. Prog. Phys.*, 2014, **77**, 076501.
8 S. H. Chun, Y. S. Chai, Y. S. Oh, D. Jaiswal-Nagar, S. Y. Haam, I. Kim, B. Lee, D. H. Nam, K.-T. Ko, J.-H. Park and K. H. Kim, *Phys. Rev. Lett.*, 2010, **104**, 037204.
9 S. Dong, J.-M. Liu, S.-W. Cheong and Z. F. Ren, *Adv. Phys.*, 2015, **64**, 519–626.
10 I. A. Sergienko and E. Dagaotto, *Phys. Rev. B: Condens. Matter Mater. Phys.*, 2006, **73**, 0944343.
11 H. Katsura, N. Nagaosa and A. V. Balatsky, *Phys. Rev. Lett.*, 2005, **95**, 057205.
12 Y. J. Choi, H. Yi, S. Lee, Q. Huang, V. Kiryukhin and S.-W. Cheong, *Phys. Rev. Lett.*, 2008, **100**, 047601.
13 H. Murakawa, Y. Onose, S. Miyahara, N. Furukawa and Y. Tokura, *Phys. Rev. Lett.*, 2010, **105**, 137202.
14 J. Z. Cong, K. Zhai, Y. S. Chai, D. S. Shang, D. D. Khalyavin, R. D. Johnson, D. P. Kozlenko, S. E. Kichanov, A. M. Abakuov, A. A. Tsirlin, L. Dubrovinsky, X. L. Xu, Z. G. Sheng, S. V. Ovsyannikov and Y. Sun, *Nat. Commun.*, 2018, **9**, 2996.
15 T. Kimura, G. Lawes and A. P. Ramirez, *Phys. Rev. Lett.*, 2005, **94**, 137201.
16 S. Ishiwata, Y. Taguchi, H. Murakawa, Y. Onose and Y. Tokura, *Science*, 2008, **319**, 1643–1646.
17 Y. Noda, H. Kimura, M. Fukunaga, S. Kobayashi, I. Kagomiya and K. Kohn, *J. Phys.: Condens. Matter*, 2008, **20**, 434206.
18 N. Hur, S. Park, P. A. Sharma, J. S. Ahn, S. Guha and S.-W. Cheong, *Nature*, 2004, **429**, 392–395.
19 Y. Tokunaga, Y. Taguchi, T. Arima and Y. Tokura, *Nat. Phys.*, 2012, **8**, 838.
20 R. C. Pullar, *Prog. Mater. Sci.*, 2012, **57**, 1191–1334.
21 T. Kimura, *Annu. Rev. Condens. Matter Phys.*, 2012, **3**, 93–110.
22 Y. Kitagawa, Y. Hiraoka, T. Hinda, T. Ishikura, H. Nakamura and T. Kimura, *Nat. Mater.*, 2010, **9**, 797–802.

23 K. Okumura, T. Ishikura, M. Soda, T. Asaka, H. Nakamura, Y. Wakabayashi and T. Kimura, *Appl. Phys. Lett.*, 2011, **98**, 212504.
24 Y. Tokunaga, Y. Kaneko, D. Okuyama, S. Ishiwata, T. Arima, S. Wakimoto, K. Kakurai, Y. Taguchi and Y. Tokura, *Phys. Rev. Lett.*, 2010, **105**, 257201.
25 S. Hirose, K. Haruki, A. Ando and T. Kimura, *Appl. Phys. Lett.*, 2014, **104**, 022907.
26 T. Aoyama, K. Yamauchi, A. Iyama, S. Picozzi, K. Shimizu and T. Kimura, *Nat. Commun.*, 2014, **5**, 4927.
27 T. Aoyama, A. Iyama, K. Shimizu and T. Kimura, *Phys. Rev. B: Condens. Matter Mater. Phys.*, 2015, **91**, 081107(R).
28 L. H. Yin, D. H. Jang, C. B. Park, K. W. Shin and K. H. Kim, *J. Appl. Phys.*, 2016, **119**, 104101.
29 X. Rocquefelte, K. Schwarz, P. Blaha, S. Kumar and J. van den Brink, *Nat. Commun.*, 2013, **4**, 2511.
30 K. Zhai, Y. Wu, S. P. Shen, W. Tian, H. B. Cao, Y. S. Chai, B. C. Chakoumakos, D. S. Shang, L. Q. Yan, F. W. Wang and Y. Sun, *Nat. Commun.*, 2017, **8**, 519.
31 N. Momozawa, M. Mita and H. Takei, *J. Cryst. Growth*, 1987, **83**, 403–409.
32 S. Ishiwata, Y. Taguchi, Y. Tokunaga, H. Murakawa, Y. Onose and Y. Tokura, *Phys. Rev. B: Condens. Matter Mater. Phys.*, 2009, **79**, 180408.
33 N. Momozawa, Y. Nagao, S. Utsumi, M. Abe and Y. Yamaguchi, *J. Phys. Soc. Jpn.*, 2001, **70**, 2724–2732.
34 S. Utsumi, D. Yoshiba and N. Momozawa, *J. Phys. Soc. Jpn.*, 2007, **76**, 034704.